FEBS

Letters

journal homepage: www.FEBSLetters.org

Structure of the quinoline N-hydroxylating cytochrome P450 RauA, an essential enzyme that confers antibiotic activity on aurachin alkaloids

Yoshiaki Yasutake [a,*], Wataru Kitagawa [a,b], Miyako Hata [a], Taiki Nishioka [b], Taro Ozaki [c,1], Makoto Nishiyama [c], Tomohisa Kuzuyama [c], Tomohiro Tamura [a,b]

[a] *Bioproduction Research Institute, National Institute of Advanced Industrial Science and Technology (AIST), 2-17-2-1 Tsukisamu-Higashi, Toyohira-ku, Sapporo 062-8517, Japan*
[b] *Graduate School of Agriculture, Hokkaido University, Kita-9, Nishi-9, Kita-ku, Sapporo 060-8589, Japan*
[c] *Biotechnology Research Center, The University of Tokyo, 1-1-1 Yayoi, Bunkyo-ku, Tokyo 113-8657, Japan*

ABSTRACT

The cytochrome P450 RauA from *Rhodococcus erythropolis* JCM 6824 catalyzes the hydroxylation of a nitrogen atom in the quinolone ring of aurachin, thereby conferring strong antibiotic activity on the aurachin alkaloid. Here, we report the crystal structure of RauA in complex with its substrate, a biosynthetic intermediate of aurachin RE. Clear electron density showed that the quinolone ring is oriented parallel to the porphyrin plane of the heme cofactor, while the farnesyl chain curls into a U-shape topology and is buried inside the solvent-inaccessible hydrophobic interior of RauA. The nearest atom from the heme iron is the quinolone nitrogen (4.3 Å), which is consistent with RauA catalyzing the N-hydroxylation of the quinolone ring to produce mature aurachin RE.
© 2013 Federation of European Biochemical Societies. Published by Elsevier B.V. All rights reserved.

1. Introduction

Antibiotics play an important role in the treatment of severe bacterial infections. Investigations into new antibiotic regimens are required because of the emergence of multi-drug resistance, as well as new pathogenic bacteria. Aurachin alkaloids are rare compounds found in nature and are composed of a quinolone ring and farnesyl chain. Two phylogenetically unrelated bacterial species, *Rhodococcus* and *Stigmatella*, are known to synthesize several molecular variations of aurachin alkaloids [1–7]. A previous study indicated that aurachins could be potent inhibitors of mitochondrial respiration because of their structural similarity with menaquinone (vitamin K₂), the sole respiratory quinone for most eubacteria [8]. The enzymes that catalyze the synthesis of menaquinone are potential targets for the development of novel antibacterial drugs [9].

Aurachin RE is an aurachin alkaloid isolated from *Rhodococcus erythropolis* JCM 6824 (Fig. 1), and it exhibits relatively strong antibiotic activity against a wide range of gram-positive bacteria [6]. Recent studies revealed that aurachin RE exhibits inhibitory activity against 1,4-dihydroxy-2-naphthoate prenyltransferase (MenA) of *Mycobacterium tuberculosis*, which is an essential enzyme in the menaquinone biosynthesis pathway [10–12]. Therefore, the antibiotic property of aurachin RE might be caused by the inhibition of menaquinone biosynthesis as well as the respiratory chain reaction itself [12]. We recently identified the operon for aurachin RE biosynthesis (*rauA–rauH*) of *R. erythropolis* JCM 6824, and gene disruption experiments revealed that *rauA*, which encodes a cytochrome P450 monooxygenase, is crucial for its antibiotic activity [7]. In addition, we found that recombinant P450 RauA catalyzes nitrogen hydroxylation of the quinolone ring and produces the mature antibiotic aurachin RE. Therefore, RauA is considered to be the final enzyme that completes the biosynthesis of aurachin RE [7]. Interestingly, the P450 gene functionally corresponding to RauA has not been found in the genome sequence of *Stigmatella aurantiaca* Sg a15 [4], and thus, RauA is likely a unique entity specifically evolved for the recognition of the aurachin skeleton in *R. erythropolis*.

P450s are heme-containing enzymes widely found in eukaryotes, bacteria, and archaea and play a role in diverse biological functions, such as biosynthesis of steroids, lipids, antibiotics, detoxification of xenobiotics, and drug metabolism [13]. A typical
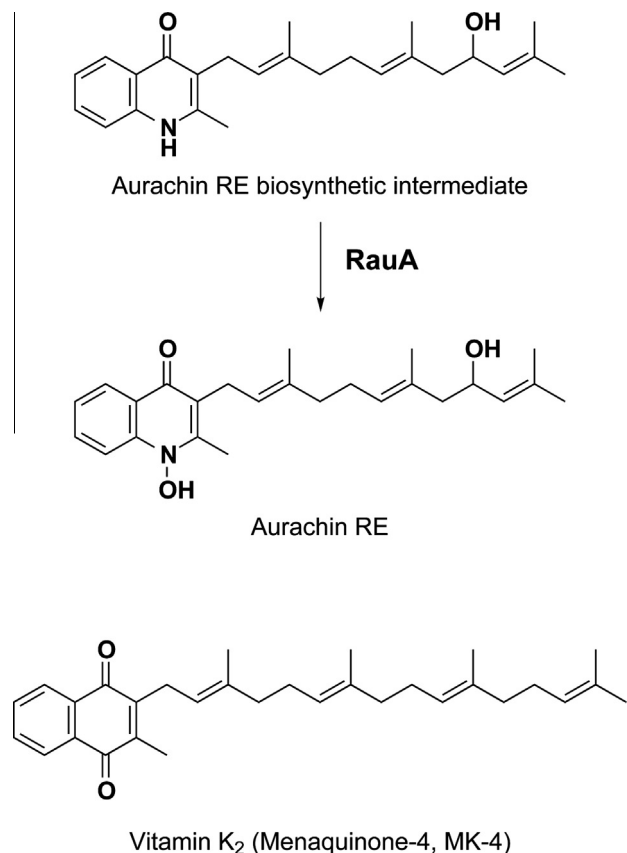

Fig. 1. Enzymatic reaction catalyzed by RauA. Aurachin RE biosynthetic intermediate is the substrate for RauA. The structure of vitamin K_2 (Menaquinone-4, MK-4) is also shown. The figure was created using ChemDraw (CambridgeSoft).

reaction catalyzed by P450s is monooxygenation, i.e., insertion of an activated oxygen atom generated from molecular oxygen (O_2) into the substrate compound using two electrons sequentially delivered from the redox partner protein and an additional two protons [14]. P450s form a conserved 3D structure known as the "P450-fold"; however, the substrate-binding pocket in the vicinity of the heme cofactor has evolved to accommodate a wide variety of compounds. In bacteria, most P450s are distributed in actinomycetes and are considered to be involved in the biosynthesis of certain secondary metabolites, including antibiotics, and metabolism of exogenous compounds. Currently, a number of P450 genes have been identified because of the recent advances in genome analysis. However, the biological function, substrate specificity, and 3D structures of most P450s remain unknown.

Here, we report the enzymatic and structural characterization of a new bacterial P450, RauA. Since aurachins are rare compounds found in nature, it is of interest to elucidate how RauA recognizes the aurachin skeleton. RauA is also unique in that it catalyzes the hydroxylation of the cyclic nitrogen atom, although some P450s are known to catalyze N-hydroxylation of amines or amidines [15,16]. Our structure clearly showed that the aurachin RE intermediate is buried inside the active-site pocket with the nitrogen atom of its quinolone moiety oriented toward the heme iron.

2. Materials and methods

2.1. Overexpression and purification of RauA

Gene cloning and analysis of recombinant protein expression were performed according to a previously described method [7]. Briefly, the *rauA* gene was cloned into the *Nde*I and *Xho*I sites of

the pET26 expression vector, and the recombinant RauA containing a C-terminal His$_6$-tag was expressed in *Escherichia coli* BL21-CodonPlus(DE3)-RIL cells. The expression of RauA was induced with 0.1 mM isopropyl β-D-thiogalactopyranoside in LB medium supplemented with $FeSO_4$ (100 μM) and 5-aminolevulinic acid (80 μg/ml) [17]. The RauA was purified by Ni-affinity chromatography followed by anion-exchange chromatography [7]. For crystallization, the purity was increased by gel-filtration chromatography with a Sephacryl S-100 column (GE-Healthcare) using a solution containing 20 mM Tris pH 7.5, 150 mM NaCl, and 10% glycerol. A carbon monoxide binding assay [18] was performed to verify the RauA concentration.

2.2. Enzyme activity measurement and kinetic analysis

Aurachin RE biosynthetic intermediate (substrate) was obtained from the culture media of *rauA* gene disruption mutant strain of *R. erythropolis* as previously described [7]. The enzyme assay was performed with reconstitution experiments. The reaction mixture contained 1.0–2.5 μM RauA, 1.0–20.0 μM substrate, 100 μg/ml spinach ferredoxin (Fdx) (Sigma–Aldrich), 0.1 U/ml spinach ferredoxin reductase (FdxR) (Sigma–Aldrich), 3 U/ml D-glucose dehydrogenase (TOYOBO), 2 mM NADPH, and 60 mM D-glucose in a total volume of 200 μl of reaction buffer (50 mM Tris–HCl, pH 7.5). After pre-incubation at 30 °C for 2 min, the reaction was initiated by the addition of NADPH, followed by incubation at 30 °C for the appropriate period (2–5 min). The reaction was terminated by extracting once with 800 μl of ethyl acetate. The resulting organic extract was dried and re-dissolved in 100 μl of methanol. The methanol solution was analyzed by HPLC (high-performance liquid chromatography) using the same procedure as previously described [7]. The molar quantity of aurachin RE and its intermediate was estimated on the basis of the previously reported molar absorption coefficient for aurachin D at one of its major absorption peaks (334 nm) [1]. The K_m and k_{cat} values were estimated from Michaelis–Menten kinetics using the KaleidaGraph (Synergy Software), after triplicate experiments with varying substrate concentrations.

2.3. Substrate binding assay

The substrate-induced spectral shift was monitored using a JASCO V-630 spectrophotometer with a 1-cm path length quartz cell. The aurachin RE intermediate (substrate) was dissolved in dimethyl sulfoxide (DMSO) at concentrations ranging from 0 to 10 μM, and 10 μl of the substrate solution was added to 990 μl of a reaction mixture containing 2.5 μM RauA and 20 mM Tris–HCl, pH 7.5. Spectral titrations with 0–10 μM substrate were performed at 25 °C. The equation $\Delta A = \Delta A_{max}([S]/([S] + K_d))$ was fitted to the experimental data using the nonlinear least squares fitting program (SOLVER; http://www.solver.com/), where [S] is the free substrate concentration. The [S] was obtained as $[S] = [S]_{total} - [ES] = [S]_{total} - ([E]\Delta A/\Delta A_{max})$, where $[S]_{total}$ is the total concentration of substrate, [ES] is the concentration of enzyme–substrate complex, and [E] is the total concentration of enzyme [19].

2.4. Crystallization

All crystallization experiments were performed at 293 K using the vapor-diffusion technique. Prior to crystallization, the protein solution was pre-incubated overnight at 277 K with a 10-fold molar excess of substrate. The protein solution was mixed with an equal volume of precipitant solution and equilibrated against the reservoir containing the same precipitant solution. RauA was crystallized using a precipitant solution containing 0.1 M MES pH

Table 1
Crystallographic parameters and refinement statistics.

Data collection statistics	
Beamline	AR-NW12A
Wavelength (Å)	1.0000
Resolution (Å)	50–2.19 (2.31–2.19)[a]
Unit-cell dimensions	
a, b, c (Å)	41.5 100.0, 52.3
α, β, γ (°)	90.0, 108.7, 90.0
Space group	$P2_1$
Observed reflections	75,296
Unique reflections	20,745
R_{merge}[b]	0.056 (0.335)[a]
Completeness (%)	99.5 (99.1)[a]
Redundancy	3.6 (3.5)[a]
Mean I/σ (I)	11.4 (3.0)[a]
Refinement statistics and model quality	
Resolution range (Å)	50–2.19
R_{work}[c]	0.214
R_{free}[d]	0.263
Total number of atoms (all/protein/heme/AUI/ solvent)[e]	3203/3078/43/28/54
Average B-factor (all/protein/heme/AUI/solvent) ($Å^2$)[e]	55.7/56.6/26.3/41.3/ 38.4
rmsd bond distances (Å)	0.013
rmsd bond angles (°)	2.39
Ramachandran plot (favored/allowed/outliers) (%)	89.4/10.6/0.0

[a] Values in parentheses refer to data in the highest resolution shell (2.31–2.19 Å).
[b] $R_{merge} = \Sigma_h \Sigma_i |I_{h,i} - \langle I_h \rangle| / \Sigma_h \Sigma_i I_{h,i}$, where $\langle I_h \rangle$ is the mean intensity of a set of equivalent reflections.
[c] $R_{work} = \Sigma |F_{obs} - F_{calc}|/\Sigma F_{obs}$ for 95% of the reflection data used in the refinement. F_{obs} and F_{calc} are observed and calculated structure factor amplitudes, respectively.
[d] R_{free} is the equivalent of R_{work}, except that it was calculated for a randomly chosen 5% test set excluded from refinement.
[e] AUI, PDB chemical identifier for aurachin RE intermediate.

6.5 and 12% PEG20000. The X-ray diffraction experiments were performed at the Photon Factory (PF) AR-NW12A using a charge-coupled device (CCD) detector (ADSC). For the X-ray diffraction study, the crystal was briefly soaked into a precipitant solution supplemented with 20% glycerol and flash-cooled in a liquid nitrogen gas stream at 100 K. The diffraction data were processed using the program iMosflm/SCALA [20,21]. The crystal belongs to the space group $P2_1$, with unit-cell dimensions a = 41.5, b = 100.0, c = 52.3 Å, α = 90.0, β = 108.7 and γ = 90.0°.

2.5. Structure determination

The structure of RauA was solved by molecular replacement with the program PHASER [22] using the atomic coordinates of the truncated P450 BioI (PDB code, 3EJD [23]) as a search model. A clear solution for one monomer in the asymmetric unit was obtained. The iterative model refinement and manual model corrections were performed using the program REFMAC5 [24] and the graphic program Coot [25]. The stereochemical quality of the final refined models was assessed using PROCHECK [26]. Molecular drawings were prepared using the program PyMOL (http://www.pymol.org/). Crystallographic parameters and model refinement statistics are summarized in Table 1. The atomic coordinates and structure factor amplitudes of RauA have been deposited in the RCSB Protein Data Bank under the accession code 3WEC.

2.6. Phylogenetic analysis

Sequences with homology to RauA were obtained from the bacterial P450 database (http://drnelson.uthsc.edu/CytochromeP450.html) or NCBI (http://www.ncbi.nlm.nih.gov/) via

the BLAST explorer. The phylogenetic tree was constructed using the Phylogeny.fr server [27] using the default settings.

3. Results and discussion

3.1. Enzyme assay and spectroscopic characterization

Firstly, we describe the results of the kinetic and spectroscopic analysis of RauA, by using the biosynthetic intermediate of aurachin RE as a substrate. The in vitro reconstituted enzyme assay was carried out with spinach ferredoxin and ferredoxin reductase as the electron donor for the recombinant RauA, and the reaction product (mature aurachin RE) was detected by HPLC analysis. The k_{cat} and K_m values were 3.97 ± 0.45 min^{-1} and 0.82 ± 0.12 μM, respectively (Supplemental Fig. 1). These values are comparable to those of other bacterial and mammalian P450s that metabolize highly hydrophobic compounds (see e.g., [17,28–32]; Supplemental Table 1). The UV–Vis spectral analysis also showed that RauA exhibited high binding affinity to the aurachin RE intermediate, with an estimated dissociation constant (K_d) of 0.12 μM (Fig. 2). High substrate binding affinity suggests that RauA is specialized for the recognition of the aurachin RE intermediate.

Binding of substrate to P450s is known to induce a change in the absorption spectrum caused by a transformation in the spin state of the heme iron. Typically, the substrate-free resting P450s are present in a low-spin ferric state, where water is coordinated to the heme iron as the sixth ligand. The water moves away when the substrate is bound, which induces a change in the spin state of the heme iron from low to high spin. Most P450s show an absorption peak (Soret peak) at around 420 nm in the low-spin state, which shifts to around 390 nm in the high-spin state: this phenomenon is known as a "type I spectral change" [33]. The absorption spectrum of RauA in the absence of the aurachin RE intermediate showed a Soret peak at 421 nm, indicating that the heme iron of the RauA is present in the typical, low-spin resting state. The addition of substrate unambiguously induced the type-I spectral change, but the absorption spectrum in the presence of a molar excess of substrate showed a broad peak from 390 to 420 nm (Fig. 2). One possible explanation is that the spin state of the heme iron is unstable and might be present as a mixture of low-spin and high-spin in the presence of the substrate. A type II spectral change can also occur when the nitrogen atom is coordinated to the heme iron as the sixth ligand [33], which is characterized by a decrease in absorption at around 400 nm accompanied by an increase at 425 nm. However, the type II spectral changes were not observed in this study.

3.2. Overall structure of RauA

The crystal structure of RauA was determined in complex with the aurachin RE intermediate (substrate) at 2.19 Å resolution. Crystallization of the substrate-free RauA was also attempted. However, it did not yield a good quality single crystal suitable for X-ray structure determination. The RauA structure was solved by molecular replacement method using the truncated atomic model of P450 BioI (CYP107H1) [23] as the search model. The asymmetric unit contains one monomer of RauA that defines the continuous electron density map, except for the 10 residues at the N-terminal and the C-terminal His-tag regions. The atomic model consists of one polypeptide-chain (residues 11–411), one heme ligand, one substrate, and 54 water molecules, and was refined with a crystallographic R factor and R_{free} factor of 21.4% and 26.3%, respectively. X-ray data collection and refinement statistics are summarized in Table 1. The structure exhibits the typical P450-fold consisting of 14 α-helices (αA, αB, αB′, αC–αM) and 8 β-strands (βA–βH)
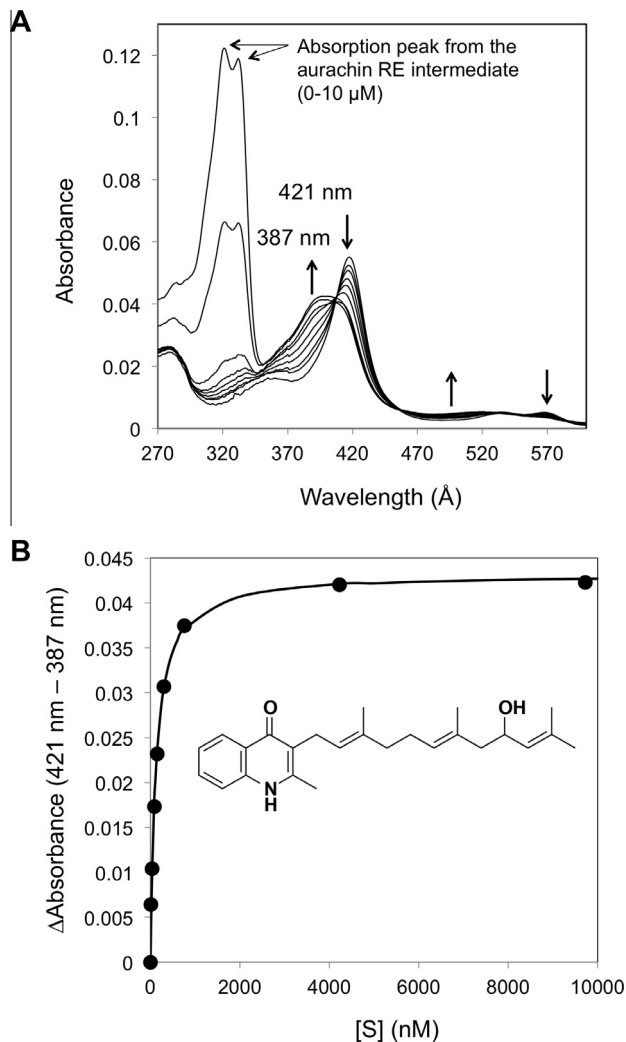
Fig. 2. Substrate-binding spectral assay. (A) Shown is the spectral change of P450 RauA upon the addition of the aurachin RE intermediate. Strong absorption peaks around 320 nm originate from the aurachin alkaloid, as previously reported [1]. (B) The best-fit titration curve to a single-binding site model is graphed. The curve was generated by nonlinear regression, as described in the materials and methods.

(Fig. 3). The overall structure is divided into two domains: the smaller β-strand rich domain and larger α-helix rich domain. The heme cofactor is embedded inside the core of the molecule—sandwiched between the distal I-helix and proximal L-helix. The heme iron is probably reduced by synchrotron radiation as observed in some studies (e.g., [34]). The propionate groups of the heme cofactor interact with the side chains of Arg305, His108, and His359. The thiol group of Cys361 is coordinated to the heme iron on the proximal side with a distance of 2.4 Å. These residues are well conserved among all P450 sequences (Supplemental Fig. 2). The highly conserved Thr and its neighboring Asp residues in the I-helix are known to be important for oxygen activation [35]. In the RauA structure, the corresponding residues are Thr257 and Glu256, respectively (Supplemental Fig. 2).

3.3. Comparison with other related bacterial P450s

We performed a structural homology search using the DALI server [36], which showed that the most structurally homologous P450 is the vitamin D_3 hydroxylase (Vdh; CYP107BR1) in an open conformation (PDB code, 3A4G) [37], with a root mean square deviation (rmsd) of 2.1 Å for the 365 Cα atoms (Z score, 44.6).
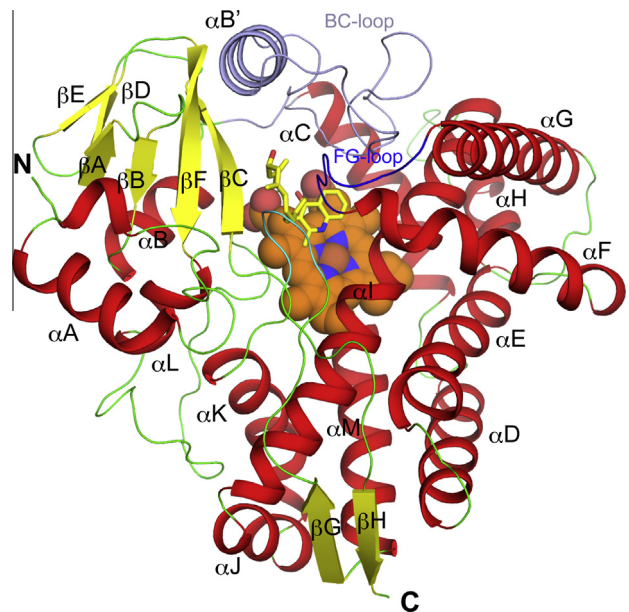

Fig. 3. Ribbon diagram of the overall structure of RauA. The α-helices and β-strands are labeled alphabetically from N- to C-terminus (αA–αM and βA–βH). The α-helices, β-strands, and loops are colored in red, yellow, and green, respectively. The heme cofactor embedded in the center of the molecule is shown as a sphere, and the bound substrate is shown as a stick model. The mobile moieties of the P450-fold, the BC-loop and FG-loop, are colored in light blue and dark blue, respectively. The C-terminal loop partially creating the substrate-binding pocket is colored in cyan.

P450 EryK (CYP113A1; PDB code, 2WIO) [38], PikC (CYP107L1; PDB code, 2BVJ) [39], and CYP164B2 (PDB code, 3R9C) [40] also show relatively high structural homology to RauA, with an rmsd ranging from 2.2 to 2.7 Å. Structure superimposition showed that the core structure of the RauA is similar to the structures of those homologous P450s (Supplemental Fig. 3); however, structural differences are also present. The most significant structural differences are located in the two loop regions—a loop between αB and αC (BC-loop) and between αF and αG (FG-loop) (Fig. 3 and Supplemental Fig. 3)—which are generally known as the mobile moieties of the P450-fold involved in substrate recognition. The curved F-helix of RauA lies across the I-helix, and its C-terminal end reaches an almost vertical position from the heme iron, with a distance of 10 Å. The polypeptide chain of the FG-loop forms an extended conformation and partly builds the substrate-binding pocket. The BC-loop region of RauA forms an additional α-helix (αB′), which is not found in the structures of Vdh, EryK, and PikC (Supplemental Fig. 3). The RauA BC-loop completely closes the gap between the β-strand rich domain and the FG-loop, and thus, the substrate-binding pocket is occluded from the solvent.

An NCBI BLAST search showed that there is one hypothetical P450 in *Streptomyces sulphureus* (SsP450; NCBI accession number, WP_016906746) with an amino acid sequence identity of 45% to RauA. Sequence identities with other higher ranked P450s are all below 33%. The BLAST search against the bacterial P450 database [41] showed that some P450s from the *Streptomyces*, *Mycobacterium*, and *Frankia* species are also homologous to RauA but with amino acid sequence identity of no more than 33%. Notably, 18 out of the top 20 sequences belong to CYP107, CYP164, or CYP233 families, with sequence identities ranging from 28% to 33%. These results suggest that RauA is located on the periphery of the CYP107/CYP164/CYP233 clusters. We constructed a phylogenetic tree with the sequences of SsP450, CYP107, CYP164, and CYP233, which revealed that RauA and SsP450 are closely related and do not overlap with the CYP107, CYP164, and CYP233 clusters
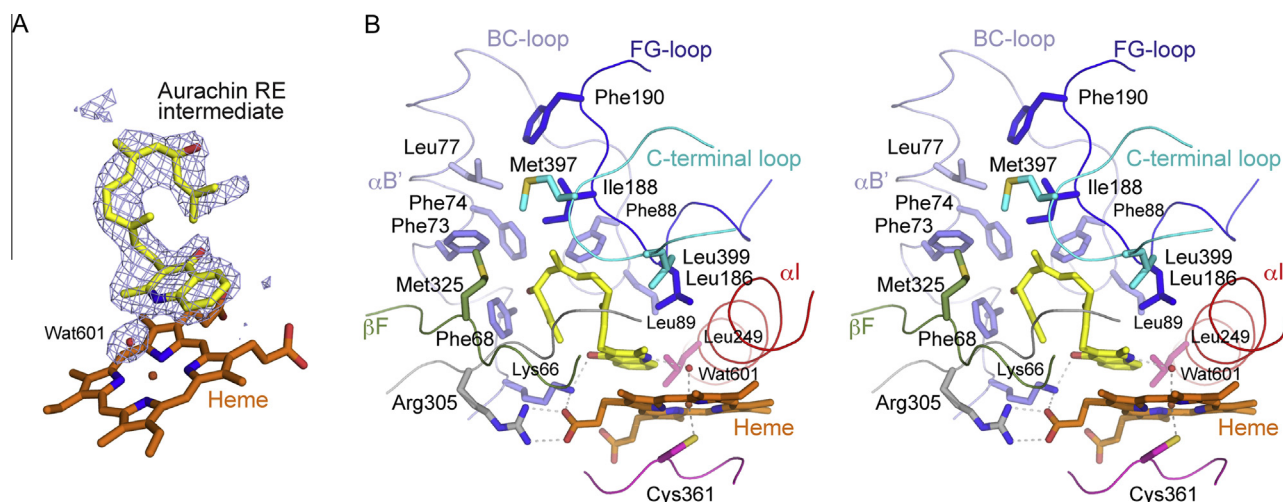
Fig. 4. Active-site structure of RauA. (A) An $mF_o−DF_c$ omit map for the bound substrate (aurachin RE intermediate) and the water molecule (Wat601) is shown. The map was contoured at a 3.2σ level. (B) Shown is the stereo-view of the active-site structure of RauA with the bound substrate (aurachin RE intermediate). Side-chains creating the highly hydrophobic active-site pocket are shown as sticks and labeled. The side-chains of Lys66 and Arg305 interacting with quinolone oxygen and heme propionate group are also shown. The models for the BC-loop, FG-loop, αI, βF, and C-terminal loop are colored in light blue, dark blue, red, green, and cyan, respectively. The proximal cysteine ligand (Cys361) is also shown in magenta.

(Supplemental Fig. 4). It is proposed that RauA and SsP450 will be classified as a clan, namely, CYP1050 (Nelson, D.R., personal communication).

3.4. Aurachin binding mode of RauA

Structural analysis showed clear electron density for the bound substrate, which fitted well to the aurachin RE intermediate model (Fig. 4A). The aurachin RE intermediate was accommodated in the highly hydrophobic active-site pocket created by the side-chains of Phe73, Phe74, Phe68, Phe88, Leu186, and Leu399 (Fig. 4B). The farnesyl chain moiety of the aurachin curled into a U-shape topology, i.e., the distance between the C12 and C24 located at each end of the farnesyl group is approximately 3.3 Å. In addition, the hydrophobic side chains of Leu77, Ile188, Phe190, Met325, and Met397 are clustered at the top of the active-site pocket, which completely closes the active-site pocket and shelters the bound substrate from the solvent. There could be another conformational state that opens the active site and is required for substrate entry and egress. The quinolone ring of the aurachin RE intermediate is located roughly parallel to the porphyrin plane of the heme via stacking interactions, with a distance of approximately 3.4 Å. The quinolone ring is also stabilized by two hydrogen bonds. One is formed between the carbonyl oxygen of the quinolone ring and the amino nitrogen of the Lys66, with a distance of 2.9 Å. The amino nitrogen of Lys66 also interacts with one of the propionate groups of the heme. The other is formed between the nitrogen of the quinolone ring and the solvent molecule (Wat601) with a distance of 3.0 Å. The solvent also interacts with the main chain oxygen of Ala253 (2.9 Å) and the heme iron (2.5 Å). The nearest quinolone atom from the heme iron is the nitrogen (4.3 Å), which is consistent with RauA catalyzing the hydroxylation of the nitrogen atom. The existence of the solvent molecule at the sixth ligand position of the heme iron is also consistent with the results of the substrate-binding spectral assay, i.e., the spin state of the heme iron did not completely shift to the high-spin state in the presence of the substrate. The hydrogen bond with substrate nitrogen atom might allow the solvent to remain as a ligand to the heme iron in the substrate-bound structure. It is generally thought that the solvent needs to move away in order for the reduction of the heme iron and subsequent molecular oxygen binding, the steps of which are crucial for initiating the

P450 catalytic cycle. Thus, there may be a hidden structural mechanism, such as a subtle local conformational change to expel the water, to promote catalytic turnover. The N-hydroxylating P450s are uncommon, and only a couple of mammalian P450s such as CYP1A2 are known to catalyze N-hydroxylation of aromatic amines. To date, several high-energy reaction intermediate models for amine N-hydroxylation have been proposed [42,43]. In contrast to these, RauA hydroxylates the nitrogen atom in the quinolone ring structure, a reaction that is geometrically distinct from the amine N-hydroxylation. The structure of RauA reported in this study may serve as an atomic model for further studies with molecular dynamics simulation and computational chemistry.

Appendix A. Supplementary data

Supplementary data associated with this article can be found, in the online version, at http://dx.doi.org/10.1016/j.febslet.2013.11.016.

References

[1] Kunze, B., Höfle, G. and Reichenbach, H. (1987) Aurachins, new quinoline antibiotics from myxobacteria: production, physico-chemical and biochemical properties. J. Antibiot. 40, 258–265.

[2] Sandmann, A., Dickschat, J., Jenke-Kodama, H., Kunze, B., Dittmann, E. and Müller, R. (2007) A type II polyketide synthase from the gram-negative bacterium *Stigmatella aurantiaca* is involved in aurachin alkaloid biosynthesis. Angew. Chem., Int. Ed. 46, 2712–2716.

[3] Nachtigall, J., Schneider, K., Nicholson, G., Goodfellow, M., Zinecker, H., Imhoff, J.F., Süssmuth, R.D. and Fiedler, H.P. (2010) Two new aurachins from *Rhodococcus* sp. Acta 2259. J. Antibiot. 63, 567–569.

[4] Pistorius, D., Li, Y., Sandmanny, A. and Müller, R. (2011) Completing the puzzle of aurachin biosynthesis in *Stigmatella aurantiaca* Sg a15. Mol. BioSyst. 7, 3308–3315.

[5] Kitagawa, W. and Tamura, T. (2008) Three types of antibiotics produced from *Rhodococcus erythropolis* strains. Microbes Environ. 23, 167–171.

[6] Kitagawa, W. and Tamura, T. (2008) A quinoline antibiotic from *Rhodococcus erythropolis* JCM 6824. J. Antibiot. 61, 680–682.

[7] Kitagawa, W., Ozaki, T., Nishioka, T., Yasutake, Y., Hata, M., Nishiyama, M., Kuzuyama, T. and Tamura, T. (2013) Cloning and heterologous expression of the aurachin RE biosynthesis gene cluster afford a novel cytochrome P-450 for quinoline N-hydroxylation. ChemBioChem 14, 1085–1093.

[8] Romagnoli, S., Oettmeier, W. and Zannoni, D. (1996) The effects of decyl aurachins C and D on the respiratory electron flow of facultative phototrophic bacteria. Biochem. Mol. Biol. Int. 39, 671–678.

[9] Kurosu, M. and Begari, E. (2010) Vitamin K_2 in electron transport system: are enzymes involved in vitamin K_2 biosynthesis promising drug targets? Molecules 15, 1531–1553.

[10] Kurosu, M., Narayanasamy, P., Biswas, K., Dhiman, R. and Crick, D.C. (2007) Discovery of 1,4-dihydroxy-2-naphthoate prenyltransferase inhibitors: new drug leads for multidrug-resistant Gram-positive pathogens. J. Med. Chem. 50, 3973–3974.

[11] Kurosu, M. and Crick, D.C. (2009) MenA is a promising drug target for developing novel lead molecules to combat *Mycobacterium tuberculosis*. Med. Chem. 5, 197–207.

[12] Debnath, J., Siricilla, S., Wan, B., Crick, D.C., Lenaerts, A.J., Franzblau, S.G. and Kurosu, M. (2012) Discovery of selective menaquinone biosynthesis inhibitors against *Mycobacterium tuberculosis*. J. Med. Chem. 55, 3739–3755.

[13] Coon, M.J., Ding, X.X., Pernecky, S.J. and Vaz, A.D. (1992) Cytochrome P450: progress and predictions. FASEB J. 6, 669–673.

[14] Munro, A.W., Grivan, H.M., Mason, A.E., Dunford, A.J. and McLean, K.J. (2013) What makes a P450 tick? Trends Biochem. Sci. 38, 140–150.

[15] Mansuy, D. (1994) Cytochrome P-450 and model systems: great diversity of catalyzed reactions. Pure Appl. Chem. 68, 737–744.

[16] Kim, D. and Guengerich, F.P. (2005) Cytochrome P450 activation of arylamines and heterocyclic amines. Annu. Rev. Pharmacol. Toxicol. 45, 27–49.

[17] Fujii, Y., Kabumoto, H., Nishimura, K., Fujii, T., Yanai, S., Takeda, K., Tamura, N., Arisawa, A. and Tamura, T. (2009) Purification, characterization, and directed evolution study of a vitamin D_3 hydroxylase from *Pseudonocardia autotrophica*. Biochem. Biophys. Res. Commun. 385, 170–175.

[18] Omura, T. and Sato, R. (1964) The carbon monoxide-binding pigment of liver microsomes. I. Evidence for its hemoprotein nature. J. Biol. Chem. 239, 2370–2378.

[19] Chen, P.-F., Berka, V., Tsai, A.-L. and Wu, K.K. (1998) Effects of Asp-369 and Arg-372 mutations on heme environment and function in human endothelial nitric-oxide synthase. J. Biol. Chem. 273, 34164–34170.

[20] Battye, T.G., Kontogiannis, L., Johnson, O., Powell, H.R. and Leslie, A.G. (2011) IMOSFLM: a new graphical interface for diffraction-image processing with MOSFLM. Acta Crystallogr., Sect. D: Biol. Crystallogr. 67, 271–281.

[21] Winn, M.D., Ballard, C.C., Cowtan, K.D., Dodson, E.J., Emsley, P., Evans, P.R., Keegan, R.M., Krissinel, E.B., Leslie, A.G., McCoy, A., McNicholas, S.J., Murshudov, G.N., Pannu, N.S., Potterton, E.A., Powell, H.R., Read, R.J., Vagin, A. and Wilson, K.S. (2011) Overview of the CCP4 suite and current developments. Acta Crystallogr., Sect. D: Biol. Crystallogr. 67, 235–242.

[22] McCoy, A.J., Grosse-Kunstleve, R.W., Adams, P.D., Winn, M.D., Storoni, L.C. and Read, R.J. (2007) Phaser crystallographic software. J. Appl. Crystallogr. 40, 674–685.

[23] Cryle, M.J. and Schlichting, I. (2008) Structural insights from a P450 carrier protein complex reveal how specificity is achieved in the P450$_{Biol}$ ACP complex. Proc. Natl. Acad. Sci. USA 105, 15696–15701.

[24] Murshudov, G.N., Skubak, P., Lebedev, A.A., Pannu, N.S., Steiner, R.A., Nicholls, R.A., Winn, M.D., Long, F. and Vagin, A.A. (2011) REFMAC5 for the refinement of macromolecular crystal structures. Acta Crystallogr., Sect. D: Biol. Crystallogr. 67, 355–367.

[25] Emsley, P., Lohkamp, B., Scott, W.G. and Cowtan, K. (2010) Features and development of *Coot*. Acta Crystallogr., Sect. D: Biol. Crystallogr. 66, 486–501.

[26] Laskowski, R.A., MacArthur, M.W., Moss, D.S. and Thornton, J.M. (1993) PROCHECK: a program to check the stereochemical quality of protein structures. J. Appl. Crystallogr. 26, 283–291.

[27] Dereeper, A., Guignon, V., Blanc, G., Audic, S., Buffet, S., Chevenet, F., Dufayard, J.F., Guindon, S., Lefort, V., Lescot, M., Claverie, J.M. and Gascuel, O. (2008) Phylogeny.fr: robust phylogenetic analysis for the nonspecialist. Nucleic Acids Res. 36, W465–W469.

[28] Uchida, E., Kagawa, N., Sakaki, T., Urushiro, N., Sawada, N., Kamakura, M., Ohta, M., Kato, S. and Inoue, K. (2004) Purification and characterization of mouse CYP27B1 overproduced by an *Escherichia coli* system coexpressing molecular chaperonins GroEL/ES. Biochem. Biophy. Res. Commun. 323, 505–511.

[29] Han, S., Choi, S., Chun, Y.-J., Yun, C.-H., Lee, C.H., Shin, H.J., Na, H.S., Chung, M.W. and Kim, D. (2012) Functional characterization of allelic variants of polymorphic human cytochrome P450 2A6 (CYP2A6*5, *7, *8, *18, *19, and *35). Biol. Pharm. Bull. 35, 394–399.

[30] Guo, J., Zhou, Y.J., Hillwig, M.L., Shen, Y., Yang, L., Wang, Y., Zhang, X., Liu, W., Peters, R.J., Chen, X., Zhao, Z.K. and Huang, L. (2013) CYP76AH1 catalyzes turnover of miltiradiene in tanshinones biosynthesis and enables heterologous production of ferruginol in yeasts. Proc. Natl. Acad. Sci. USA 110, 12108–12113.

[31] Johnston, J.B., Ouellet, H. and Ortiz de Montellano, P.R. (2010) Functional redundancy of steroid C_{26}-monooxygenase activity in *Mycobacterium tuberculosis* revealed by biochemical and genetic analyses. J. Biol. Chem. 285, 36352–36360.

[32] Wang, Q., Hillwig, M.L., Okada, K., Yamazaki, K., Wu, Y., Swaminathan, S., Yamane, H. and Peters, R.J. (2012) Characterization of CYP76M5-8 indicates metabolic plasticity within a plant biosynthetic gene cluster. J. Biol. Chem. 287, 6159–6168.

[33] Schenkman, J.B., Remmer, H. and Estabrook, R.W. (1967) Spectral studies of drug interaction with hepatic microsomal cytochrome. Mol. Pharmacol. 3, 113–123.

[34] Beitlich, T., Kühnel, K., Schulze-Briese, C., Shoeman, R.L. and Schlichting, I. (2007) Cryoradiolytic reduction of crystalline heme proteins: analysis by UV–Vis spectroscopy and X-ray crystallography. J. Synchrotron Rad. 14, 11–23.

[35] Nagano, S. and Poulos, L. (2005) Crystallographic study on the dioxygen complex of wild-type and mutant cytochrome P450cam: implications for the dioxygen activation mechanism. J. Biol. Chem. 280, 31659–31663.

[36] Holm, L. and Sander, C. (1995) Dali: a network tool for protein structure comparison. Trends Biochem. Sci. 20, 478–480.

[37] Yasutake, Y., Fujii, Y., Nishioka, T., Cheon, W.K., Arisawa, A. and Tamura, T. (2010) Structural evidence for enhancement of sequential vitamin D_3 hydroxylation activities by directed evolution of cytochrome P450 vitamin D_3 hydroxylase. J. Biol. Chem. 285, 31193–31201.

[38] Savino, C., Montemiglio, L.C., Sciara, G., Miele, A.E., Kendrew, S.G., Jemth, P., Gianni, S. and Vallone, B. (2009) Investigating the structural plasticity of a cytochrome P450: three-dimensional structures of P450 EryK and binding to its physiological substrate. J. Biol. Chem. 284, 29170–29179.

[39] Sherman, D.H., Li, S., Yermalitskaya, L.V., Kim, Y., Smith, J.A., Waterman, M.R. and Podust, L.M. (2006) The structural basis for substrate anchoring, active site selectivity, and product formation by P450 PikC from *Streptomyces venezuelae*. J. Biol. Chem. 281, 26289–26297.

[40] Agnew, C.R., Warrilow, A.G., Burton, N.M., Lamb, D.C., Kelly, S.L. and Brady, R.L. (2012) An enlarged, adaptable active site in CYP164 family P450 enzymes, the sole P450 in *Mycobacterium leprae*. Antimicrob. Agents Chemother. 56, 391–402.

[41] Nelson, D.R. (2009) The cytochrome P450 homepage. Human Genomics 4, 59–65.

[42] Shamovsky, I., Ripa, L., Börjesson, L., Mee, C., Nordén, B., Hansen, P., Hasselgren, C., O'Donovan, M. and Sjö, P. (2011) Explanation for main features of structure–genotoxicity relationships of aromatic amines by theoretical studies of their activation pathways in CYP1A2. J. Am. Chem. Soc. 133, 16168–16185.

[43] Ji, L. and Schüürmann, G. (2013) Model and mechanism: N-hydroxylation of primary aromatic amines by cytochrome P450. Angew. Chem., Int. Ed. 52, 744–748.